Natural convection in a reservoir induced by periodic thermal forcing at the water surface

***Yadan Mao**

State Key Laboratory of Geological Processes and Mineral Resources, Institute of Geophysics and Geomatics, China University of Geosciences, Wuhan 430074, China

*Corresponding author: yadan_mao@cug.edu.cn

Abstract

Natural convection in nearshore waters induced by differential heating has significant biological and environmental impact. The present investigation is concerned with natural convection in a reservoir model induced by periodic thermal forcing at the water surface. A semi-analytical approach coupled with scaling analysis and numerical simulation is adopted to resolve the problem. The scales for temperature and flow velocity, as well as the time lag of flow response to the thermal forcing have been derived. These derived scales have been verified by results from numerical simulations. Flow response at different stages of the periodic forcing has been illustrated through snapshots of isotherms and streamlines. The phase delay of the flow response to the thermal forcing decreases as the length of period increases.

Keywords: Natural convection, Buoyant boundary layers, Scaling analysis, Semi-analytical solution, Numerical simulation, Periodic thermal forcing,

Introduction

As the depth of water increases in the offshore direction, when subject to the same rate of daytime heating or nighttime cooling, the shallow water near shore experiences larger temperature variations than that that in offshore regions. This generates a horizontal temperature gradient that drives a circulation across shore, often referred to as a 'thermal siphon'. Field observations (Adams and Wells, 1984; Monismith *et al*. 1990; 2006) have demonstrated the significance of this buoyancy driven flow in promoting water exchanges across shore. It is revealed that this thermal siphon plays the dominant role in driving cross-shore circulation in calm nearshore regions with limited wind-driven or tidal circulation, substantially reducing the residence of nearshore water bodies.

This convective circulation plays an important role in the transport of nearshore nutrients or pollutants (James and Barko, 1991; Niemann *et al*., 2004), and therefore has significant biological and environmental implications. These have motivated a series of theoretical investigations to quantify it. For the daytime heating case, the asymptotic solutions (Farrow & Patterson 1994) and scaling analysis (Lei and Patterson, 2002; Mao *et al*., 2009) provide important insight into natural convection induced by absorption of radiation. For the nighttime surface cooling case, Horsch and Stefan (1988) established an approximate relation between the flow rate and the Rayleigh number through numerical simulations and laboratory experiments. Later, through scaling analysis, detailed scaling has been derived for the cooling case (Lei and Patterson, 2005; Mao *et al.*, 2010).

All the above theoretical investigations have been conducted for constant thermal forcing. For the case of diurnally varying thermal forcing, the asymptotic solution (Farrow 2004) has been derived under the assumption that the daytime radiation energy and nighttime heat loss is uniformly distributed over the local water depth. A diurnal thermal forcing model more relevant to field situations was realized in the numerical simulations of Lei and Patterson (2006). However, no

scaling analysis is yet available for natural convection generated by diurnal thermal forcing. This has motivated the present study, which focuses on natural convection generated by periodic thermal forcing at the water surface.

Model formulation

A two-dimensional (2D) model with water depth varying with offshore distance is adopted to capture the basic mechanism of the cross-shore exchange flow. A 2D reservoir consisting of one section with a sloping bottom with a slope of *A* and the other section with a uniform depth is considered (Figure 1). With the Boussinesq assumption, the normalized 2D Navier-Stokes and energy equations governing the flow and temperature evolution are written as:

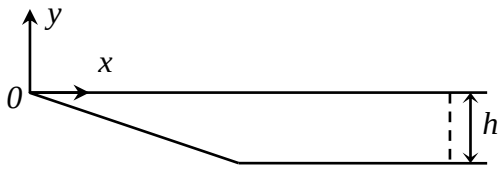

Figure 1 Sketch of the flow domain and the coordinate svstem.

$$\frac{\partial u}{\partial x}+\frac{\partial v}{\partial y}=0, \tag{1}$$

$$\frac{\partial u}{\partial t}+u\frac{\partial u}{\partial x}+v\frac{\partial u}{\partial y}=-PrRa\frac{\partial p}{\partial x}+Pr\nabla^2 u, \tag{2}$$

$$\frac{\partial v}{\partial t}+u\frac{\partial v}{\partial x}+v\frac{\partial v}{\partial y}=-PrRa\frac{\partial p}{\partial y}+Pr\nabla^2 v+PrRa\tau, \tag{3}$$

$$\frac{\partial \tau}{\partial t}+u\frac{\partial \tau}{\partial x}+v\frac{\partial \tau}{\partial y}=\nabla^2\tau. \tag{4}$$

where *Pr* and *Ra* are Prandtl number and Rayleigh number respectively, defined as:

$$Pr=\nu/\kappa, \quad Ra=g\beta\Delta T h^3/(\nu k) \tag{5}$$

The parameters g, κ, ν, β are the acceleration due to gravity, thermal diffusivity, kinematic viscosity and thermal expansion coefficient of the fluid at a reference temperature T_0, respectively. The respective scales for the normalization are: the length scale x, $y \sim h$; the time scale $t \sim h^2/\kappa$; the velocity scale u, $v \sim \kappa/h$; and the pressure gradient scale p_x, $p_y \sim \rho_0 g\beta\Delta T$. The non-dimensional temperature τ is defined as $(T-T_0)/\Delta T$. Temperature at the water surface $T_{y=0}$ is varying periodically:

$$T_{y=0}=T_0+\Delta T\sin(2\pi t/P) \tag{6}$$

The water surface is assumed to stress free ($\partial u/\partial y=0$, v=0), whereas, the bottom is assumed adiabatic ($\partial\tau/\partial\hat{n}=0$) and no-slip ($u$=0, v=0). An open boundary condition is considered for the endwall ($\partial u/\partial x=0$, v=0, $\partial\tau/\partial x=0$) with a backflow at the reference temperature T_0. The water body is initially set to be stationary and isothermal.

Theoretical analysis

Under an isothermal water surface, the vertical temperature gradient is much larger than the horizontal temperature gradient, and therefore vertical conduction dominates over horizontal conduction. Initially, the flow velocity is small and, thus, convection is also small. If convection and

horizontal conduction are neglected, the problem can be simplified as a one-dimensional conduction problem with a variable local water depth of *Ax*:

$$\frac{\partial \tau}{\partial t} = \frac{\partial^2 \tau}{\partial y^2} \tag{7}$$

$$\tau = \sin\left(2\pi t / P\right) \quad (y = 0), \tag{8}$$

$$\frac{\partial \tau}{\partial y} = 0 \quad (y = -Ax), \tag{9}$$

$$\tau = 0 \quad (t = 0). \tag{10}$$

An isothermal water surface and an adiabatic bottom are specified by (8) and (9), respectively. Equation (9) is the leading order approximation of $\partial\tau/\partial\hat{n} = 0$ under the assumption of small bottom slope *A*. An isothermal initial condition is embodied in (10). The above equations can be solved through separation of variables, and the solution of (7-10) is

$$\tau = \sin\left(\frac{2\pi}{P}t\right) + \sum_{n=0}^{\infty} \frac{32A^2x^2\cos\left(2\pi t/P\right)}{(2n+1)^3 P\pi^2}\left(1 - e^{-\frac{(n+1/2)^2\pi^2}{A^2x^2}t}\right)\sin\frac{\left(n+1/2\right)\pi}{Ax}y. \tag{11}$$

Given sufficient length of time, the exponential term approaches zero. n = 0 is the dominant term. Therefore the temperature can be simplified as:

$$\tau = \sin\left(\frac{2\pi}{P}t\right) + \frac{32A^2x^2}{\pi^2 P}\sin\left(\frac{\pi y}{2Ax}\right)\cos\left(\frac{2\pi}{P}t\right), \tag{12}$$

The non-dimensional temperature τ averaged over the local depth can be obtained from equation (12):

$$\bar{\tau} = \frac{1}{Ax}\int_{-Ax}^{0} \bar{\tau}\, dy \approx \sin\left(\frac{2\pi}{P}t\right) - \frac{64A^2x^2}{P\pi^3}\cos\left(\frac{2\pi}{P}t\right) \approx \sqrt{1 + \left(\frac{64A^2x^2}{P\pi^3}\right)^2}\,\sin\left(\frac{2\pi}{P}t - \theta\right) \tag{13}$$

where θ is the phase delay of the vertically-averaged temperature,

$$\theta \sim \arctan\left(\frac{64A^2x^2}{\pi^3 P}\right), \tag{14}$$

Following the same procedure described in Mao *et al*. (2012), a balance between buoyancy induced pressure gradient and viscous terms in the momentum equations yields the following scaling for velocity:

$$u \sim \frac{128RaA^5x^4}{\pi^3 P}\cos\left(\frac{2\pi t}{P} - \theta\right). \tag{15}$$

The above derivation is conducted under the assumption that convection is negligible and therefore applies only to the conductive region. As revealed by Mao *et al.* (2009, 2010), even for high *Ra* number flow regime, there is a nearshore conductive subregion, and the scope of this subregion shrinks landward as *Ra* increases. In the following verification of the above scaling results, the data is selected within the nearshore conductive region.

Numerical simulations

The normalized equation (1)-(4) are solved numerically using a finite-volume method. The SIMPLE (semi-implicit method for pressure-linked equations) scheme is adopted for pressure-velocity coupling; and the QUICK (quadratic upstream interpolation for convective kinematics)

scheme is applied for spatial derivatives. A second-order implicit scheme is applied for time discretization in calculating the transient flow.

The simulation is conducted with a non-dimensional depth of 1, a bottom slope of A=0.1, a horizontal length of L = 20, and a fixed Prandtl number of Pr = 7. The section with a uniform depth is set to be of the same length as the sloping section. The numerical simulation is conducted for ten full thermal forcing cycles to minimize the start-up effect.

Verification for scaling

The verification of scaling results is conducted with respect to both the magnitude and the phase delay. The maximum velocity u_{max} over the local depth is obtained for each x. Time series of u_{max} is plotted in Figure 2(a, c) for different horizontal positions and different periods respectively. It is clear that the start-up effect is only noticeable within the first cycle. If there were no phase delay θ, the velocity would reach a maximum at the start of a cycle as indicated by the cosine sign in scaling (15). However, this maximum is delayed due to the phase lag. Phase lag obtained from simulation is plotted against the scaling result in figure 2(b, d), where a clear linear relation is identified, and therefore the dependency of phase lag on x and P predicted by scaling (15) is verified.

Figure 2(a, c) shows that the maximum horizontal velocity within the cooling phase is smaller than that within the heating phase. During the heating phase, the circulation is clockwise with the surface layer flowing horizontally offshore and the bottom layer flowing up long the slope, and thus the maximum horizontal velocity u_{max} is obtained within the surface layer (Mao *et al*. 2009). During the cooling phase, the circulation is anticlockwise and the surface layer flows landward and bottom layer flows down the slope (Mao *et al*. 2010), and therefore, u_{max} is obtained within the bottom layer. As the intensity of thermal forcing during the cooling phase is the same as the heating phase, the absolute value of velocity is the same, but the direction is opposite. This reveals that the absolute value of u in the bottom layer is smaller than that in the surface layer.

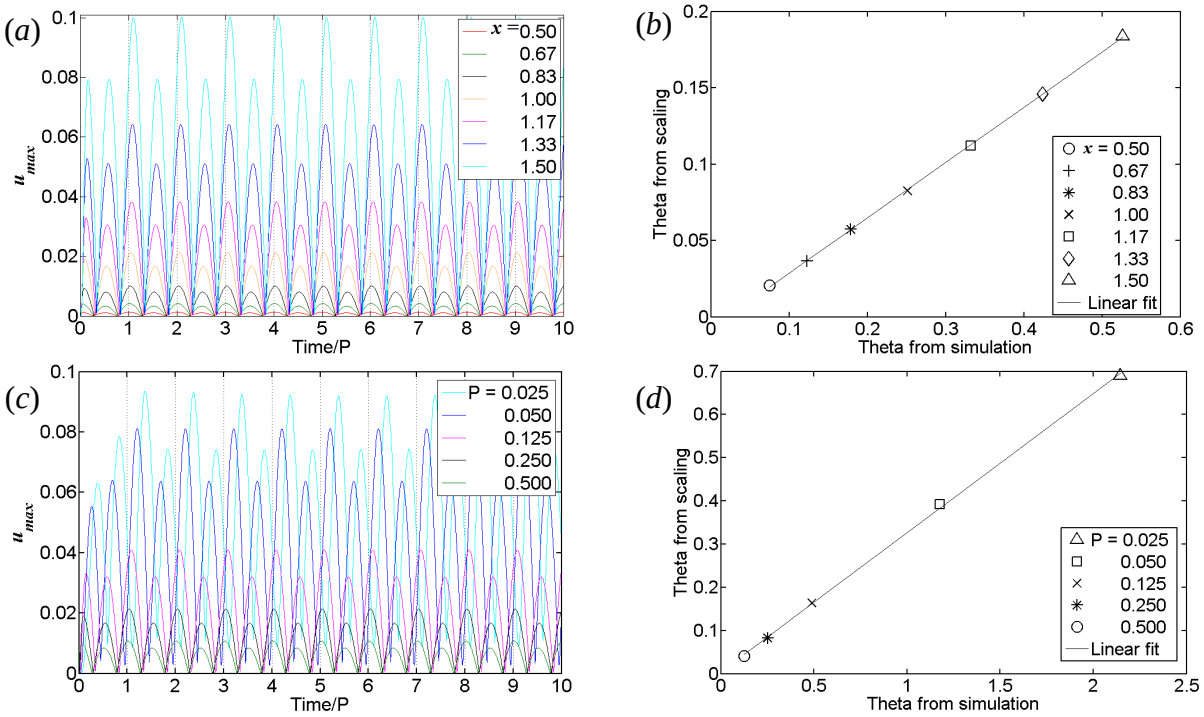

Figure 2 Verification of the phase delay θ in scaling (14), $Ra = 10^4$. (a) Time series of u_{max} at different x with P=0.25 (b) θ at different x from simulation versus scaling. (c) Time series of u_{max} under different P with x = 1.0. (d) θ under different P from simulation versus scaling.

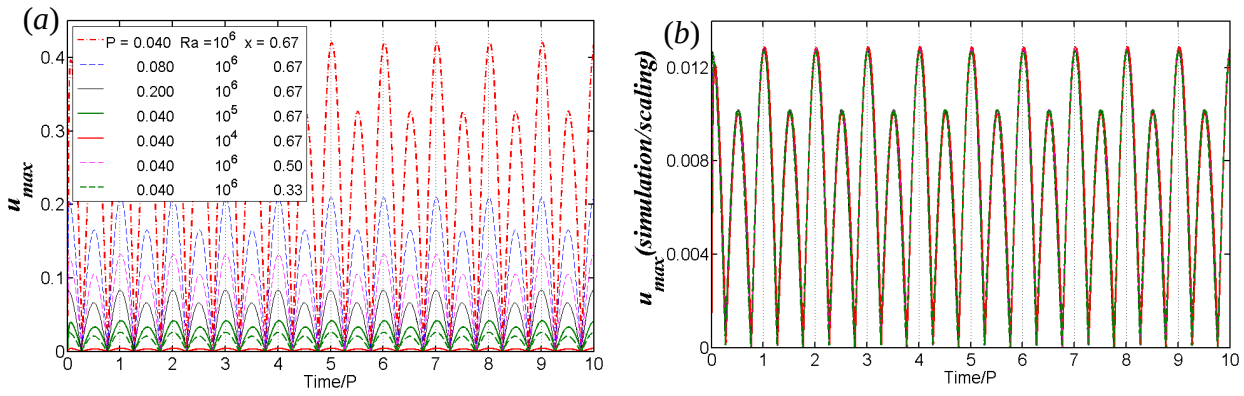

Figure 3 Verification of the dependency of u_{max} on x, P and Ra, (a) Time series of u_{max} at various P, Ra and x obtained from simulation. (b) Simulation results normalized by scaling.

The dependency of the magnitude of u_{max} on the period P, Ra and the horizontal position x predicted by scaling (15) is verified by the results of numerical simulations (Figure 3). Since the focus is on the magnitude, the effect of phase delay is minimized by selecting relatively large P and small x as scaling (14) suggests. Figure 3(a) shows the time series of the maximum horizontal velocity u_{max} for various P, Ra and x. It is clear that the amplitude of u_{max} increases with Ra and x, and decreases with P. After normalization by scaling (15), simulation results collapse together (Figure 3b), confirming the dependency of the magnitude of u_{max} on P, Ra and x.

Flow response from simulation

To illustrate the overall flow response over the entire domain, isotherms and streamlines obtained from simulation for $Ra = 10^5$, $P = 0.04$ are plotted in figure 4 over a cycle. The times shown in this figure are relative to the beginning of the cycle. Details of flow response are described below.

Before the start of the cycle ($t = 0.00P$), temperature at the water surface has been increasing for the last quarter of a cycle. Therefore, at the beginning of the cycle, a water surface layer is formed below the water surface (figure 4a). The isotherms in figure 4a suggest that a cool gravity current is expected to flow down the sloping bottom, which is confirmed in the streamlines in figure 4a, an anticlockwise flows is formed within the domain. The wavy feature in the streamlines is caused by the instability in the last quarter of a cycle. This effect of instability is counteracted by stratification caused by warm surface water at t = 0.10P as shown by the streamline in figure 4b. The isotherms of 4b suggest that the warm surface layer grows thicker. Compared to figure 4a, the horizontal temperature gradient which drives the flow is smaller in figure 4b and therefore flow velocity decreases as confirmed by the streamlines. At time $t = 0.25P$, the warm surface layer becomes even thicker, and the flow becomes even more stratified, as a result, the velocity continue to decrease as shown by the streamlines in figure 4c. Near the tip of flow domain, a conductive subregion is observed where the warm surface layer reaches the sloping bottom as shown by the isotherms. The negative horizontal temperature gradient near shore leads to a clockwise circulation as shown in the streamlines (figure 4c).

From time $t = 0.25P$, temperature at the water surface starts to decrease, as a results, the warm surface layer disappears at $t = 0.50P$ (Figure 4d). The surface layer becomes cooler than the layer below, which is potentially unstable. The clockwise flow expands to a larger scope as shown by the streamlines (figure 4d). After time $t = 0.50P$, temperature at the water surface continues to decrease, eventually lead to instabilities with cold thermal plumes plunging down the water surface at time t = 0.75P (Figure 4e).

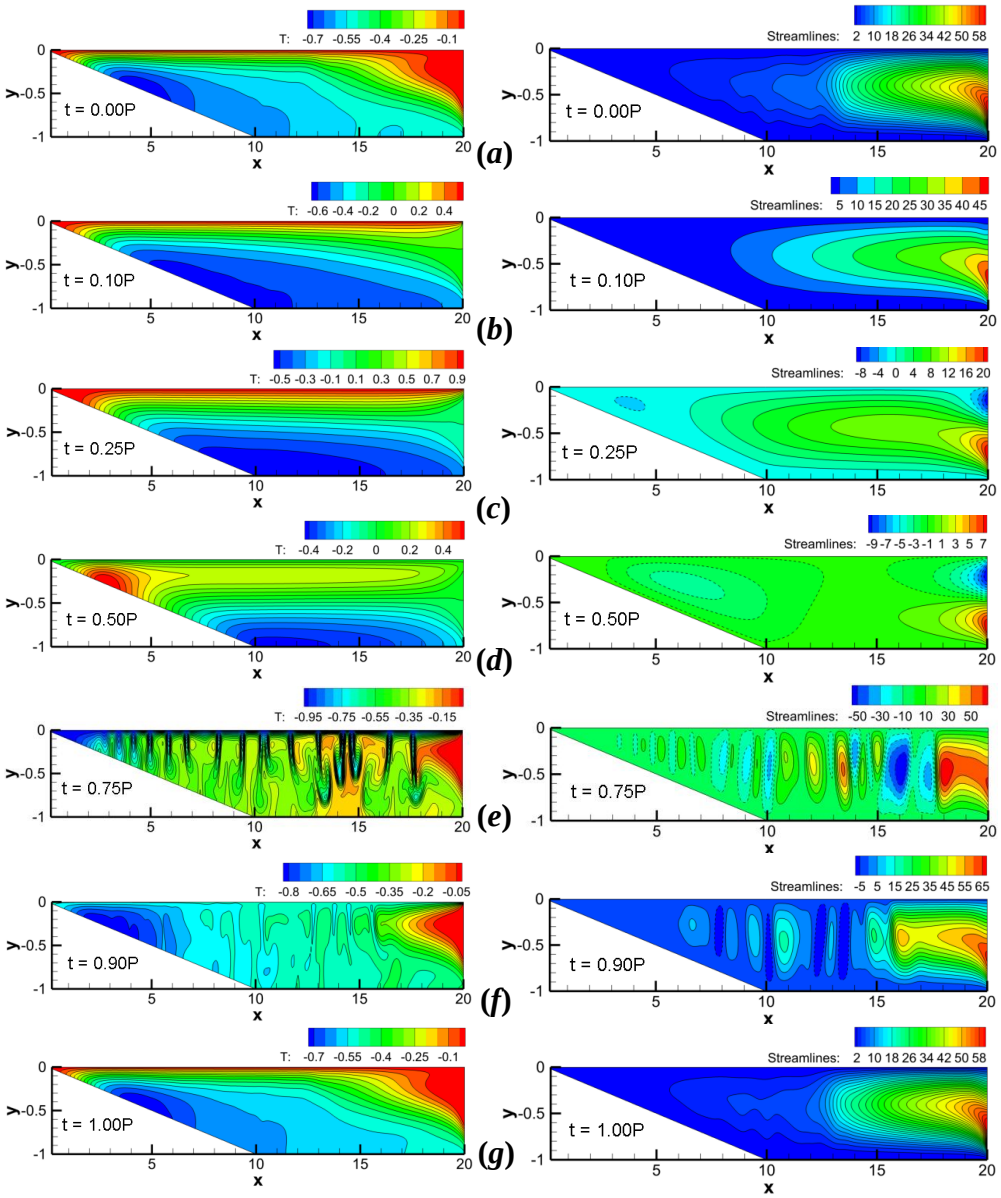

Figure 4 Flow responses to periodic thermal forcing at the water surface ($Ra = 10^5$, $P = 0.04$). Left: temperature contours. Right: streamlines. Dashed streamlines indicates clockwise flow.

After t = 0.75*P*, temperature at the water surface starts to increase, as a results, the circulation at time t = 0.90*P* is less unstable with decreased intensity of plumes (figure 4f). When the cycle finishes at t = 1.00*P*, the plunging plumes disappear and flow becomes less unstable. The end of the cycle at t = 1.00*P* is also the start of the next cycle. Since simulation is conducted over 10 full thermal forcing cycles, the effect of start-up flow is minimized. Therefore, features of the isotherms and streamlines at the end of the cycle t = 1.00*P* (figure 4*g*) is the same as at the beginning of the cycle t = 0.00*P* (figure 4*a*).

To quantify the intensity of horizontal exchange flow rate at a specified location *x*, the horizontal exchange rate $Q(x)$ at position *x* is calculated for the 2D domain as:

$$Q(x) = \frac{1}{2}\int_{-h_x}^{0} |u|\, dy, \tag{16}$$

where h_x is the local water depth at the horizontal position *x*. The average volumetric horizontal flow rate *Q* is obtained by integrating $Q(x)$ horizontally over a length of *L*:

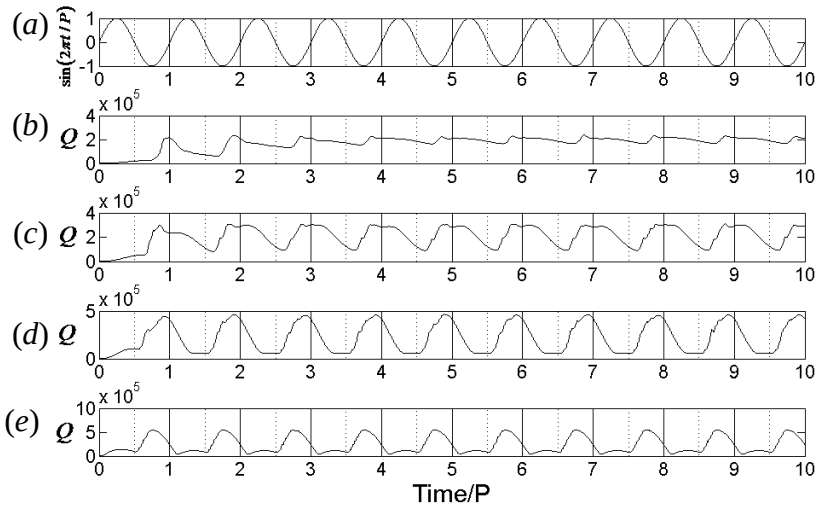

Figure 5 Flow response to periodic thermal forcing represented by the time series of Q for different period, Ra =10^6. Plotted are (a) time series of thermal forcing. (b-e) are time series of Q. (b) P = 0.004 (c) P = 0.008 (d) P = 0.020 (e) P = 0.080

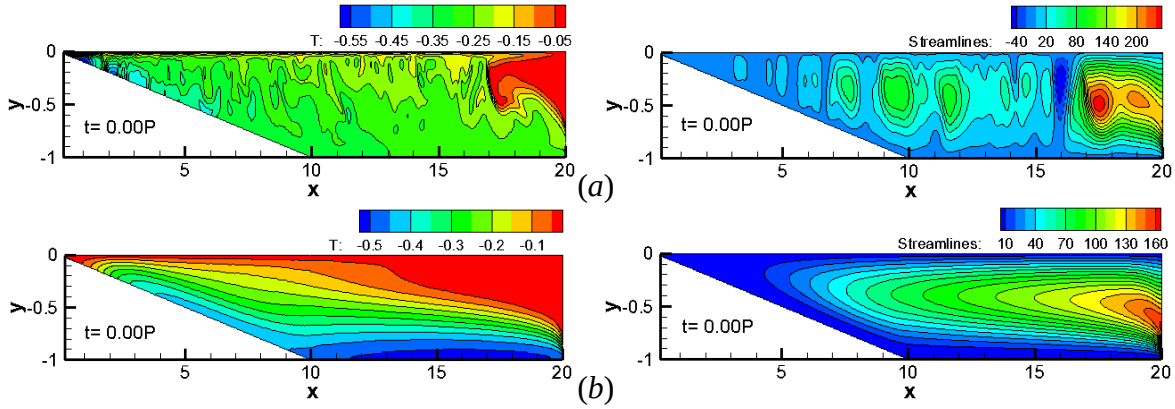

Figure 6 Isotherms and streamlines at the beginning of the cycle, Ra = 10^6. (a) P = 0.004 (b) P = 0.08. Left: temperature contours. Right: streamlines.

$$Q = \frac{1}{L}\int_0^L Q(x)dy \tag{17}$$

Figure 5 plots the time series of Q for different periods with Ra = 10^6. Time series of thermal forcing is shown in figure 5(a). The corresponding Q shown in figure 5(b-e) reveals that the length of period significantly affects the flow response. Given an isothermal domain, Q induced by surface heating (positive value in figure 5a) is expected to be much smaller than by surface cooling (negative value in figure 5a). During heating time, horizontal exchange is only induced by the horizontal temperature gradient near shore (figure 4c). During the cooling time, the thermal plumes induced by instability enhance the horizontal exchange rate significantly (figure 4e). Therefore, if there is no inertia and the flow responds instantly to the thermal forcing, a low value of Q is expected for the heating phase and a high value for the cooling phase. However, the flow response is delayed due to inertia as shown in figure 5. For short period, the delay of response is most evident. As shown in figure 6 (a), at the start of heating phase (t = 0.00 P), the flow is still unstable for the short period (P = 0.004), whereas it becomes stable for the long period (P = 0.080) which has sufficient time to respond to the varying thermal forcing. As a result, the delay is minimized for the largest period (P = 0.08) in figure 5(e), where the low and the high value of Q correspond well with the heating and the cooling phase with only a slight time delay.

Conclusions

The present investigation focuses on natural convection induced by periodic thermal forcing at the water surface in a reservoir model. Through coupled analytical solutions and scaling analysis, temperature and velocity scales for the near shore conductive region have been derived and verified by numerical simulations. The scaling quantifies the dependency of velocity on *Ra*, *A*, *x*, and *P*, and the dependency of phase delay on *A*, *x* and *P*.

The flow response over the entire domain is revealed by isotherms and streamlines at different stages of the thermal forcing cycle. An effect of phase delay is observed and the details of flow response are analyzed. Time series of horizontal exchange rate *Q* for different lengths of period *P* reveals that the length of period affects flow response significantly. The phase delay of flow response resulting from inertia is most evident in the result of the shortest period. As the length of period increases, this delaying effect becomes less obvious. For sufficiently large period, the heating and cooling phase of the thermal forcing is characterized by low and high values of *Q* respectively.

Acknowledgement

This research was supported by National Science Foundation of China (grant number 11002127) and the Fundamental Research Fund for National University, China University of Geosciences (Wuhan).

References

Adams, E. E. and Wells, S. A. (1984), Field Measurements on Side Arms of Lake. *J of Hydraul. Engng. ASLE* 110, pp. 773-793.

Farrow D. E. and Patterson J. C. (1993), On the response of a reservoir sidearm to diurnal heating and cooling, *J. Fluid Mech*. 246, pp. 143-161.

Farrow D. E. (2004), Periodically forced natural convection over slowly varying topography, *J. Fluid Mech.* 508, pp. 1-21.

Horsch G. M. and Stefan H. G. (1988), Convective circulation in littoral water due to surface cooling, *Limnol. Oceanogr.*, 33, pp. 1068-1083.

James W. F. and Barko J. W. (1991), Estimation of phosphorus exchange between littoral and pelagic zones during nighttime convective circulation, *Limnol. Oceanogr.*, 36, pp. 179-187.

Lei C. and Patterson J. C. (2002), Unsteady natural convection in a triangular enclosure induced by absorption of radiation, *J. Fluid Mech*., 460, pp. 181-209.

Lei C. and Patterson J. C. (2005), Unsteady natural convection in a triangular enclosure induced by surface cooling, *Int. J. of Heat Fluid Fl.*, 26, pp. 307-321.

Lei C. and Patterson J. C. (2006), Natural convection induced by diurnal heating and cooling in a reservoir with slowly varying topography, *JSME Int. J. B-Fluid T.*, 49, pp. 605-615.

Mao Y., Lei C. and Patterson J. C. (2009), Unsteady natural convection in a triangular enclosure induced by absorption of radiation – a revisit by improved scaling analysis, *J. Fluid Mech*., 622, pp. 75-102.

Mao Y., Lei C. and Patterson J. C. (2010), Unsteady near-shore natural convection induced by surface cooling, *J. Fluid Mech.*, 642, pp. 213-233.

Monismith S. G., Imberger J. and Morison M. L. (1990), Convective motions in the sidearm of a small reservoir, Limnol. Oceanogr., 35, pp. 1676-1702.

Monismith S. G., Genin A., Reidenbach M. A., Yahel G. and Koseff J. R. (2006), Thermally driven exchanges between a coral reef and the adjoining ocean, *J. Phys. Oceanogr*., 36, pp. 1332-1347.

Niemann H., Richter C., Jonkers H. M. and Badran M. I. (2004), Red sea gravity currents cascade near-reef phytoplankton to the twilight zone, *Mar. Ecol.-Prog. Ser*., 269, pp. 91-99.